Biomed Microdevices (2012) 14:25–33
DOI 10.1007/s10544-011-9582-y

Inertial migration of cancer cells in blood flow in microchannels

Tatsuya Tanaka · Takuji Ishikawa · Keiko Numayama-Tsuruta · Yohsuke Imai · Hironori Ueno · Takefumi Yoshimoto · Noriaki Matsuki · Takami Yamaguchi

Published online: 6 September 2011
© Springer Science+Business Media, LLC 2011

Abstract The circulating tumor cell test is used to evaluate the condition of breast cancer patients by counting the number of cancer cells in peripheral blood samples. Although microfluidic systems to detect or separate cells using the inertial migration effect may be applied to this test, the hydrodynamic forces acting on cancer cells in high hematocrit blood flow are incompletely understood. In the present study, we investigated the inertial migration of cancer cells in high hematocrit blood flow in microchannels. The maximum hematocrit used in this study was about 40%. By measuring the cell migration probability, we examined the effects of cell–cell interactions, cell deformability, and variations in cell size on the inertial migration of cancer cells in blood. The results clearly illustrate that cancer cells can migrate towards equilibrium positions up to a hematocrit level of 10%. We also performed simple scaling analysis to explain the differences in migration length between rigid particles and cancer cells as well as the effect of hematocrit on cancer cell migration. These results will be important for the design of microfluidic devices for separating cells from blood.

Keywords Inertial migration · Cancer cells · Red blood cells · Cell separation · Microchannel

T. Tanaka (✉) · T. Ishikawa · Y. Imai · T. Yoshimoto
Department of Bioengineering and Robotics,
Graduate School of Engineering, Tohoku University,
6-6-01, Aoba, Aramaki, Aoba-ku,
Sendai 980-8579, Japan
e-mail: tatsuya@pfsl.mech.tohoku.ac.jp

K. Numayama-Tsuruta · T. Yamaguchi
Department of Biomedical Engineering,
Graduate School of Biomedical Engineering, Tohoku University,
6-6-01 Aoba, Aramaki, Aoba-ku,
Sendai 980-8579, Japan

H. Ueno
International Advanced Research
and Education Organization, Tohoku University,
6-6-01 Aoba, Aramaki, Aoba-ku,
Sendai 980-8579, Japan

N. Matsuki
Department of Biomedical Engineering,
Graduate School of Engineering, Okayama University of Science,
1-1 Ridai-cho, Kita-ku,
Okayama 700-0005, Japan

1 Introduction

The number of breast cancer patients is increasing in many developed countries. In the diagnosis of breast cancer patients, it is crucial to accurately detect metastasis or recurrence of the cancer at an early stage. Recently, the circulating tumor cell (CTC) test has been widely adopted for evaluating the prognosis or cure effect of breast cancer (Cristofanilli et al. 2004; Cristofanilli et al. 2005; Budd et al. 2006). In this test, the patient's condition is evaluated by counting the number of cancer cells in a peripheral blood sample. Identification or separation of cancer cells from the other blood cells is necessary, and the accuracy of the CTC test is strongly dependent on the precision of cell identification or separation.

Many separation techniques are available for micrometer-scale particles and cells, such as fluorescence-activated cell sorting (FACS), magnetic sorting, and dielectrophoresis (Gossett et al. 2010; Pratt et al. 2011). Although these techniques are effective, they require long processing times, complex preparation procedures, and large spaces for the apparatus. To overcome these problems, microfluidic systems, which use hydrodynamic forces to separate rigid particles or cells, have been developed. One type of

microfluidic system uses inertia-induced migration of particles to separate various rigid particles based on their size (Bhagat et al. 2009; Carlo 2009; Park et al. 2009). The throughput of this method is significantly high, and the time required for particle separation is often much shorter than in other methods.

Recently, some groups have succeeded in detecting or separating different types of cells using the inertial migration effect. Kuntaegowdanahalli et al. (2009) separated SH-SY5Y neuroblastoma cells (~15 μm) from C6 rat glioma cells (~6 μm) in a dilute suspension of cells (volume fraction of about 0.05%). In their experiment, two types of inertial force were induced, i.e., the shear-induced inertial lift force and Dean force due to the centrifugal effect. Wu et al. (2009) isolated bacteria from a dilute suspension of human blood cells (about 1% hematocrit (Hct)) using inertial forces. Hur et al. (2010) sorted red blood cells (RBCs) and white blood cells (WBCs) at certain spanwise positions in the microchannel by using the inertial migration effect. As their sample was sufficiently dilute, they could recognize the type of cells by image analysis. Carlo et al. (2008) used similar inertial force-based methods to Kuntaegowdanahalli et al. (2009), and isolated platelets from other blood cells in a dilute suspension.

Although these previous studies succeeded in detecting or separating target cells from other cells, none investigated the effects of cell–cell interactions in non-dilute suspensions. In the case of cancer cell isolation from a blood sample, it is preferable to use large hematocrit blood samples to reduce the total separation time. In high hematocrit blood flow, however, the mixing effect due to RBC–RBC interactions becomes dominant, as described in our previous studies (Lima et al. 2008b; Saadatmand et al. 2011), and cancer cells may not show inertial migration. Thus, it is important to clarify the effects of cell–cell interactions on the inertial migration in high hematocrit blood samples. Moreover, the theoretical understanding of the inertial migration of cells is poor compared with that for rigid particles. Cells usually show variation in size and shape and viscoelastic rheological properties. How these characteristics affect the inertial migration remains unclear.

To address these questions, we investigated the inertial migration of cancer cells in high hematocrit blood flow. We fabricated microchannels to observe cancer cell behavior in blood samples with various hematocrit values under a large flow velocity condition. The maximum hematocrit used in this study was about 40%. By measuring the cell migration probability, we examined the effects of cell–cell interactions, cell deformability, and variation in cell size on the inertial migration of cancer cells in blood. We also performed simple scaling analysis to explain the experimental results, which will be useful in the design of microfluidic devices for cell separation.

2 Methods

2.1 Experimental setup

The experimental setup used is shown in Fig. 1(a). The experimental apparatus primarily consisted of an inverted microscope (IX71; Olympus, Tokyo, Japan) and a high-speed camera (Phantom v7.1; Vision Research, Wayne, NJ). Microchannels were placed on the stage, and the sample was injected using a syringe pump (IC 3101; KD Scientific, Holliston, MA). Images of cell motion were taken with the high-speed camera and recorded on a desktop PC.

Schematic representations of the microchannels are shown in Fig. 1(b). Two types of microchannel were fabricated: channel A was made for observing rigid microspheres or cancer cells in dilute suspensions, while channel B was made for collecting cancer cells from a high-hematocrit suspension of RBCs. A strong inertial force was induced on the particles flowing in the narrow test section, where the particle Reynolds number was large. Particle Reynolds number is defined as $\mathrm{Re}_p = \rho d^2 \dot{\gamma}/\mu$, where ρ is the density, d is the diameter, $\dot{\gamma}$ is the shear rate, and μ is the viscosity. The test section of channel A had a width of 80 μm, height of 220 μm, and length L that was varied from 0.5 cm to 2.0 cm. To facilitate image analysis, the width of the microchannel was expanded to 450 μm upstream and downstream of the test section. The test section of channel B was 70 μm in width, 270 μm in height, and 1.5 cm in length. The outlet channel was split into three branches, and samples in regions of different widths were collected separately. These microchannels were fabricated by soft lithography with a protocol similar to that used in our previous study (Lima et al. 2008a). In brief, the mold of channel was fabricated on a silicon wafer with negative photoresist (SU-8 2075; Kayaku MicroChem, Tokyo, Japan). The PDMS (Silpot 184; Dow Corning, Midland, MI) was prepared by mixing a commercial prepolymer and catalyzerat a weight ratio of 10:1. The mixture was poured on the mold master and cured by baking for about 40 min at 85°C. After peeling the PDMS from the master, fluidic ports were punched by using a puncher (BIOPSY PUNCH; Kai Industries, Gifu, Japan). Irreversible bonding of the PDMS microchannel to a glass slide was achieved using oxygen plasma treatment.

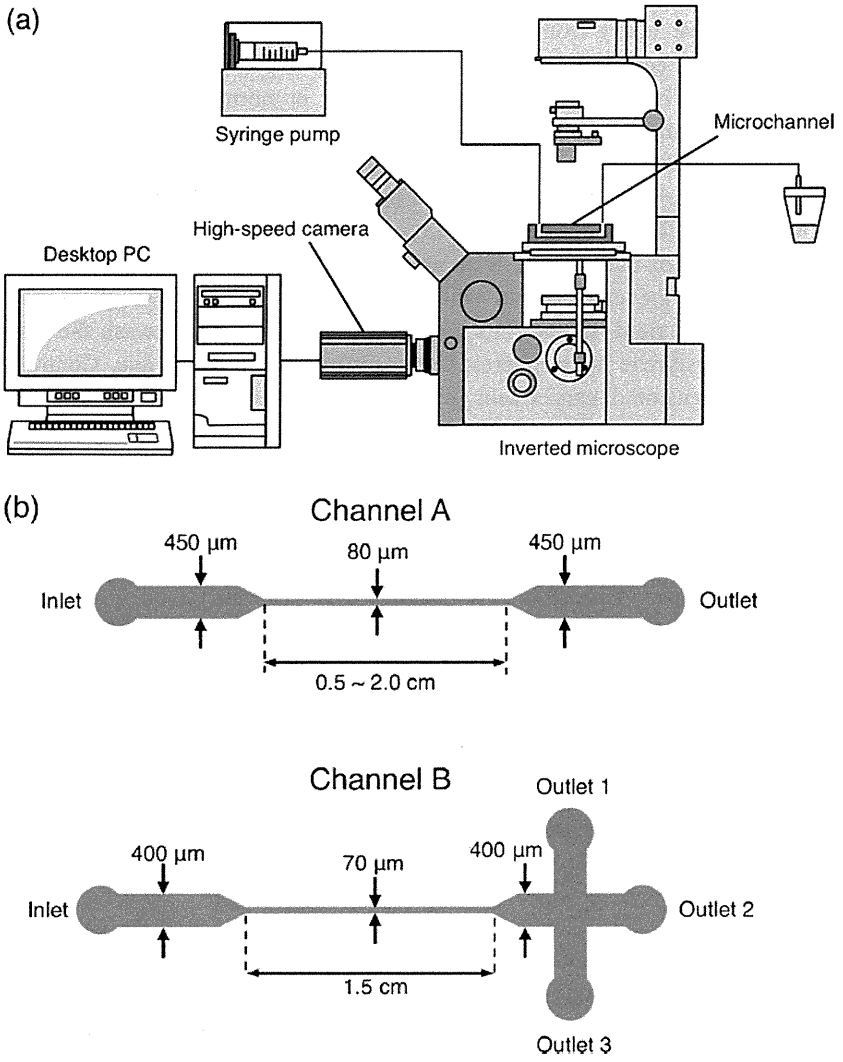

Fig. 1 Experimental setup. (**a**) Schematic representation of the experimental setup. (**b**) Geometries of two types of PDMS microchannel. The heights of channel A and B are 220 μm and 270 μm, respectively

2.2 Materials

The poorly differentiated human breast cancer cell line MDA-MB-231 was used in this study. The diameter distribution of cancer cells and their number density in the suspension were measured using a cell counter (Vi-CELL XR Cell Viability Analyzer; Beckman Coulter Inc., Brea, CA). The average diameter of cells was about 15 μm with a standard deviation of about 4.3 μm (Fig. 2). Cells were cultured in 25-cm^2 tissue culture flasks, and maintained in RPMI 1640 (Invitrogen Corp., Carlsbad, CA) with 10% fetal bovine serum (FBS; Thermo Fisher Scientific Inc., Waltham, MA) and 1× antibiotic-Antimycotic (Invitrogen) at a temperature of 37°C with 5% CO_2 (cf. Ishikawa et al. 2011). In each experiment, cells were grown to 80–90% confluence, and harvested from the tissue culture flasks by adding 0.25% trypsin–EDTA (Invitrogen) and dissociated. The cells were then used in the experiments after washing twice with Dulbecco's phosphate buffered saline (D-PBS (−)) (Invitrogen).

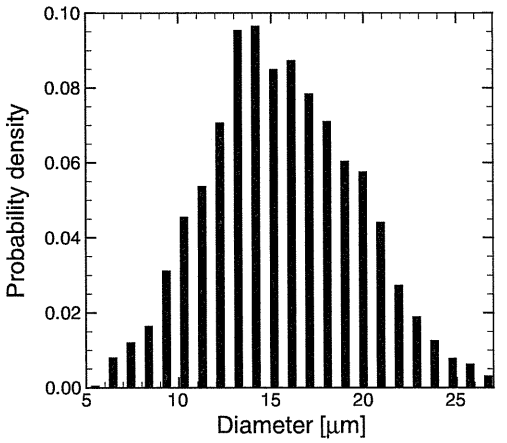

Fig. 2 Probability density distribution of the diameter of cancer cells

RBCs were taken from healthy 25–38-year-old male volunteers and centrifuged to separate the RBCs and other constituents. The RBCs were then preserved in normal saline at 4°C and resuspended in Dextran 40 prior to each experiment. All procedures were carried out in compliance with the guidelines of the Clinical Investigation Ethics Committee at Tohoku University.

Three types of fluid sample were used in this study. Two were used in the experiments with channel A: a dilute suspension of rigid spheres 15 μm in diameter (Fluo-Spheres polystyrene microspheres; Invitrogen) in PBS, and a dilute suspension of cancer cells (MDA-MB-231) in PBS. The concentrations of both rigid spheres and cancer cells were about 1×10^5 particles or cells per mL. The density and the viscosity of PBS at 25°C were 1.05×10^3 kg/m^3 and 1.15×10^{-3} Pa·s, respectively. The third fluid was used in the experiments with channel B: a non-dilute suspension of cancer cells and RBCs in 5% Dextran 40 (DEX40) solution, in which DEX40 (low density Dextran L 10% w/v in lactated Ringer's solution; Otsuka Pharmaceutical Co. Ltd., Tokyo, Japan) was diluted by the same volume of lactated Ringer's solution (Otsuka Pharmaceutical). The density and viscosity of the 5% DEX40 solution at 25°C were 1.01×10^3 kg/m^3 and 1.99×10^{-3} Pa·s, respectively. The Hct of RBCs ranged from 0.1% to 40%, and the ratio of cancer cells to RBCs was set to about 0.2% to 0.8%, where cell–cell interactions between cancer cells were negligible.

2.3 Experimental procedures

In the experiments with channel A, the behaviors of rigid spheres and cancer cells were observed on the upstream and downstream sides of the test section. The flow rate was controlled by a syringe pump in the range 64–256 μL/min, corresponding to a particle Reynolds number of about 0.16–0.62. To analyze particle behavior, probability densities of the width position from the center were calculated by the following equation:

$$P_i = \left(\sum_{j=1}^{M} n_{i,j}\right) \Big/ \left(\sum_{j=1}^{M}\sum_{i=1}^{N} n_{i,j}\right) \quad (1)$$

where P_i is the probability density at section i, M is the total number of frames recorded with 40-ms interval, and $n_{i,j}$ is the number of particles in section i at frame j. The half width of the channel was split into 50 sections (i.e., N=50) and each section was 4.5 μm in width. More than 100 particles were counted to calculate the probability density in each experiment.

In the experiments with channel B, the flow rate was fixed at Re_p=0.6. It is difficult to count the number of cancer cells suspended in high Hct blood by image analysis. Instead, we used a flow cytometer (JSAN; Bay Bioscience, Hyogo, Japan) to count the number of nuclear stained cancer cells in concentrated suspensions of RBCs. After the experiment, samples taken from each outlet were prepared according to the following protocol: precipitate cells from the DEX40 solution by centrifugation; add 2 μL of 100-fold diluted DRAQ5 (Cell Signaling Technology Inc., Danvers, MA) solution and 98 μL of PBS to the samples; mix gently and incubate for 20 min at 4°C; and wash the samples twice with fresh PBS to remove excess dye. Control tests were also performed using non-labeled samples. The number of labeled cells (i.e., nucleated cancer cells) per 10^5 cells was determined by measuring the fluorescence intensity of cells.

3 Results

3.1 Migration of rigid spheres in PBS

To confirm the usefulness of the designed microchannels, the behavior of rigid spheres in PBS was investigated. Figure 3 shows the probability density of the width position of rigid spheres at the inlet and outlet with Re_p=0.622. The probability density at the inlet was almost uniform, while that at the outlet showed a large peak around 125 μm from the center (i.e., 100 μm from the wall). This result was consistent with those of Bhagat et al. (2009), who reported that particles migrated at about $0.4W_c$ away from the sidewalls, where W_c was the half-width of the test section.

The effects of particle Reynolds number, Re_p, and the length of the test section L were also investigated, and the results are shown in Fig. 4. By decreasing Re_p, the probability of rigid spheres moving toward the equilibrium position was decreased (Fig. 4(a)). When Re_p=0.156,

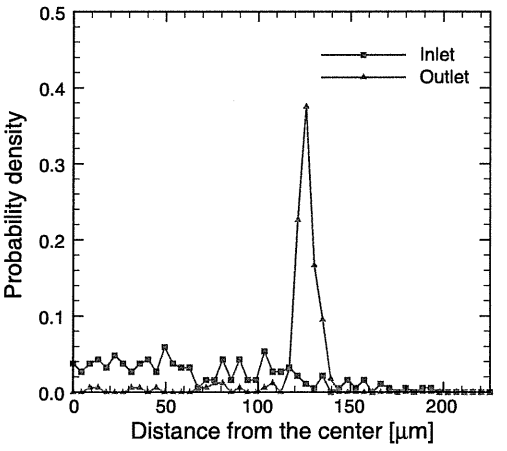

Fig. 3 Probability density of the width position of rigid spheres at the inlet and the outlet with Re_p=0.622. The wall is located 225 μm from the center in channel A

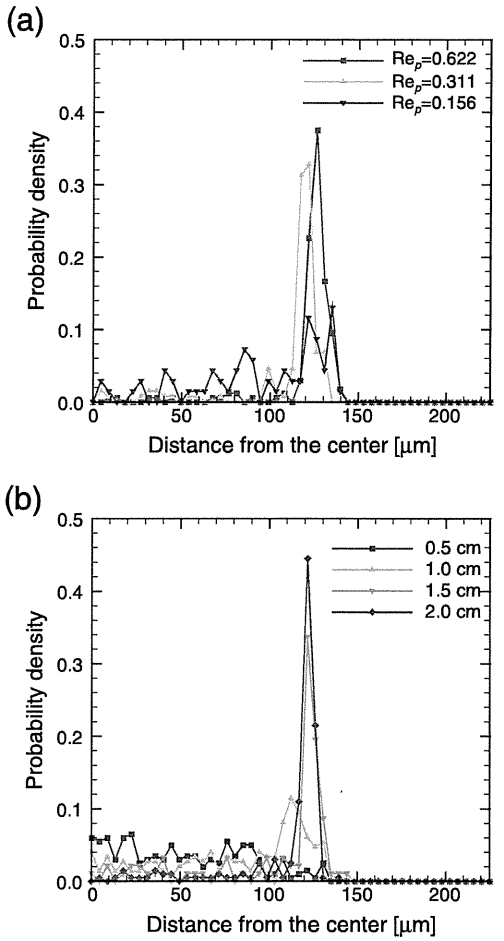

Fig. 4 Probability density of the width position of rigid spheres at the outlet: (**a**) effect of particle Reynolds number Re_p (L=1.0 cm); and (**b**) effect of the channel length L (Re_p=0.156)

migration of rigid spheres was not clearly observed. In Fig. 4(b), the migration of rigid spheres was not significant when L=0.5 or 1.0 cm, whereas migration was apparent when L=1.5 or 2.0 cm. These results indicated that migration of the rigid spheres was due to an inertial effect. Large values of Re_p and L are necessary to achieve strong migration of particles. These results were consistent with those of previous studies (Bhagat et al. 2009; Carlo 2009; Park et al. 2009).

3.2 Migration of cancer cells in PBS

Next, the migration of cancer cells in PBS was investigated to clarify the differences between the rigid spheres and biological cells. Figure 5 shows the probability density of the width position of cancer cells at the inlet and the outlet with Re_p=0.622. Similar to rigid spheres, the probability density of cancer cells at the inlet was almost homogeneous, whereas that at the outlet showed a large peak around 115 μm from the center (i.e., 110 μm from the wall).

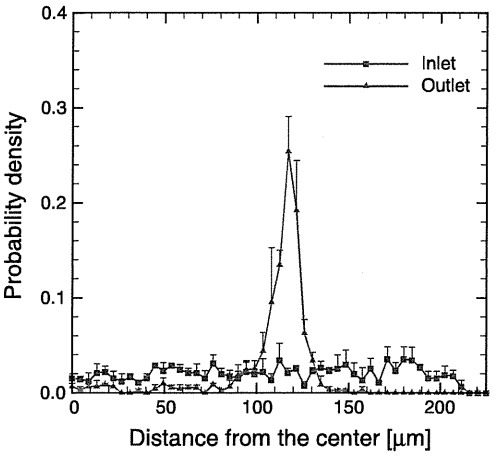

Fig. 5 Probability density of the width position of cancer cells at the inlet and the outlet with Re_p=0.622. *Error bars* indicate standard deviations. The wall is located 225 μm from the center in channel A

The maximum probability density of cancer cells was not as high as that of rigid spheres, and the probability density function was slightly blunter than that of rigid spheres.

The effects of Re_p and L on the probability density of cancer cells are shown in Fig. 6. The peak in the probability density became higher as Re_p was increased (Fig. 6(a)). When Re_p=0.156, migration of cancer cells was not clearly observed, similar to the case for rigid spheres (cf. Fig. 4(a)). In the cases of L=1.5 and 2.0 cm (Fig. 6(b)), obvious migration of cancer cells was observed. These basic tendencies were the same between the rigid spheres and cancer cells.

To examine differences in migration properties between the rigid spheres and cancer cells quantitatively, we normalized all experimental results using the migration length L_m. L_m can be defined for rigid spheres by considering the balance of forces between the shear-induced migration force and the viscous drag force, as described by Bhagat et al. (2009):

$$L_m = \frac{3\pi\mu}{2\rho U}\left(\frac{W_c}{a}\right)^3, \tag{2}$$

where U is the average velocity in the test section, W_c is the half width of the test section, and a is the radius of the rigid sphere. When L is much larger than L_m, most of the particles migrate at the equilibrium positions. When L is much smaller than L_m, on the other hand, most of the particles remain at their original width positions. To quantify the migration strength in each experiment, we calculated the maximum probability densities of six sections, $PD_{6,\,max}$, defined by:

$$PD_{6,\max} = \left[\sum_{i}^{i+5} P_i\right]_{\max}, (i = 1 - 45) \tag{3}$$

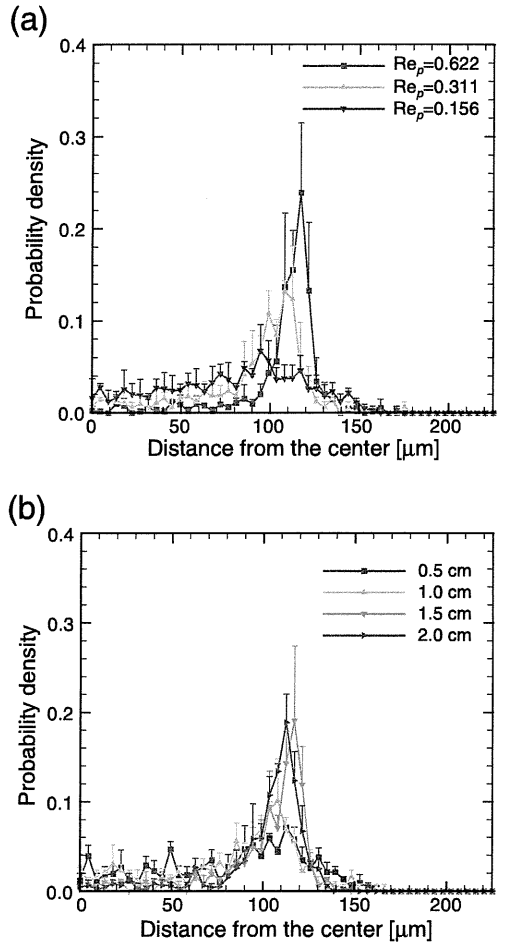

Fig. 6 Probability density of the width position of cancer cells at the outlet. (**a**) Effect of particle Reynolds number Re_p (L=1.0 cm). (**b**) Effect of the channel length L (Re_p=0.311). *Error bars* indicate standard deviations

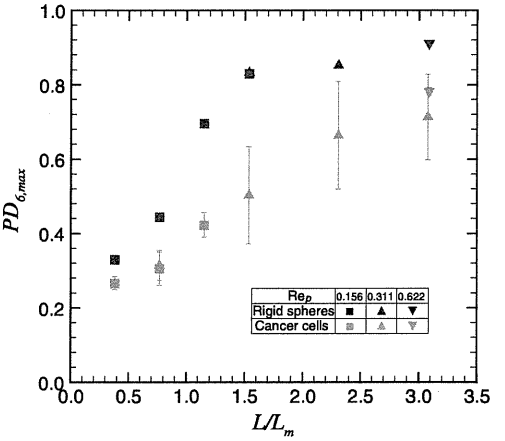

Fig. 7 Correlations between $PD_{6,\ max}$, defined by Eq. 3, and the normalized channel length L/L_m. The figure contains all experimental data using channel A under the conditions of Re_p=0.16–0.62 and L=0.5–2.0 cm. *Error bars* indicate standard deviations

where max indicates the maximum value. A large value of $PD_{6,\ max}$ indicates that large numbers of rigid spheres or cancer cells were focused in the narrow band in the width direction.

Figure 7 shows the correlation between L/L_m and $PD_{6,\ max}$. All results of the present study are plotted in the figure, and thus the results cover experimental conditions of Re_p= 0.16–0.62 and L=0.5–2.0 cm. The results for rigid spheres and cancer cells were markedly different, and the cancer cells required a longer channel length than the rigid spheres to reach the equilibrium state.

3.3 Migration of cancer cells in RBC suspension

To clarify the effect of RBCs on the migration of cancer cells, we performed experiments under various Hct conditions, 0.1%, 1%, 10%, and 40% Hct, in which the ratio of cancer cells to RBCs was less than 0.8%. In this section, channel B was used, and particle Reynolds number was fixed as Re_p=0.6. Samples were taken from each outlet, and the number of labeled cells (i.e., cancer cells) was counted by flow cytometry. Figure 8 shows the fluorescence intensity plots of samples taken from outlets 1 and 3, and outlet 2 under conditions of 1% Hct. The graph is divided into four areas, where the lower left area indicates non-labeled cells (i.e., RBCs) and the upper right area indicates labeled cells (i.e., cancer cells). The sample taken from outlet 2 had a considerably smaller number of cancer cells than that taken from outlets 1 and 3. This result indicated that cancer cells migrated towards the equilibrium positions even in the presence of RBCs.

When the concentration of RBCs is very high, the mixing effect due to cell–cell interactions becomes dominant, and cancer cells may not show inertial migration. In this study, the effect of Hct on migration efficiency was evaluated by introducing the collection efficiency (CE) of cancer cells, defined by the following equation:

$$CE = \frac{n_{out1} + n_{out3}}{n_{out1} + n_{out2} + n_{out3}}, \tag{4}$$

where $n_{out\ i}$ is the number of cancer cells per 10^5 cells taken from outlet i. A large value of CE indicates that many cancer cells migrated near the wall and were collected from outlets 1 and 3. If cancer cells are distributed homogeneously in the suspension, i.e., $n_{out1} = n_{out2} = n_{out3}$, we have CE=2/3. The results of CE with Hct=0.1%–40% are shown in Fig. 9. In the cases of Hct=0.1%–10%, the collection efficiency of cancer cells was more than 80%. These results indicated that cancer cells were able to migrate toward the wall even with the disturbed flow generated by the RBC motions up to Hct=10%. When Hct=40%, however, the CE value was about 50%, and cancer cells did not show any inertial migration. CE may have become less than 66%

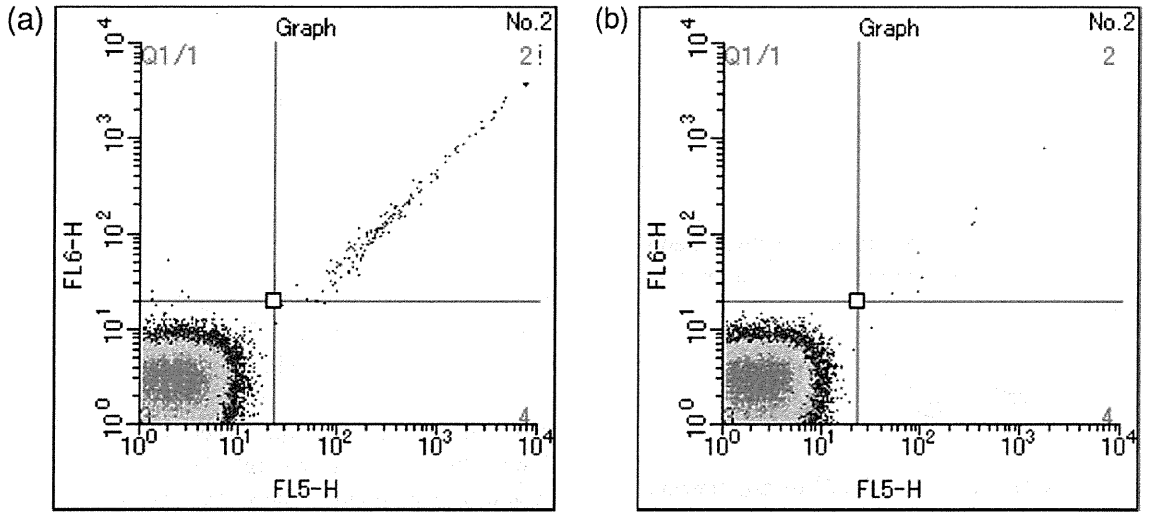

Fig. 8 Fluorescence intensity of samples taking from (**a**) outlets 1 and 3, (**b**) outlet 2 of channel B (Hct=1%). The horizontal axis (FL5-H) indicates the fluorescence intensity of cells, the wavelength of which ranged from 668 to 722 nm. The *vertical axis* (FL6-H) indicates the fluorescence intensity above a wavelength of 748 nm

because the concentration of cells near the wall was lower than that near the center, and the suspension was actually inhomogeneous in the width direction at the outlet. In the case of Hct=40%, the inertial migration effect was overwhelmed by the mixing effect due to cell–cell interactions between RBCs and cancer cells.

4 Discussion

The migration length L_m is an important quantity because it provides useful information for the design of microfluidic devices for cell separation. The theory of migration length for rigid spheres is well established, and we confirmed that the theory could predict the inertial migration of rigid spheres (Fig. 7). The migration length of cancer cells, however, was almost double that of rigid spheres (Fig. 7), and the conventional theory was not sufficiently accurate.

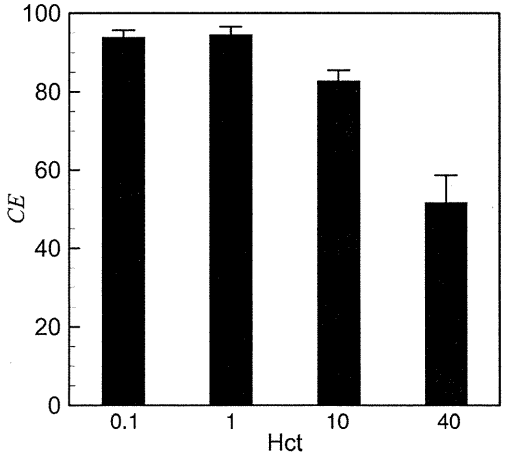

Fig. 9 Changes in the collection efficiency *CE*, defined by Eq. 4, with Hct (Channel B). *Error bars* indicate standard deviations. Where average number of $n_{out1}+n_{out3}$ and n_{out2} in Hct=0.1, 1, 10, 40% are 956, 59 (Hct 0.1%), 580, 36 (Hct 1%), 991, 200 (Hct 10%), 314, 285 (Hct 40%), respectively

There are two possible factors that may affect the difference in migration length between rigid spheres and cancer cells. The first is the deformability of cancer cells, and the other is the variation in size of cancer cells. To discuss the effects of cell deformability, we introduce capillary number, defined as $\mathrm{Ca} = \mu\dot{\gamma}/E$, where E is the Young's modulus. The Young's modulus of typical breast cancer cells is about 10^2 Pa (Lee and Lim 2007; Suresh 2007), and the fluid viscosity is in the order of 10^{-3} Pa·s. Thus, Ca becomes greater than unity only when the shear rate $\dot{\gamma}$ becomes higher than 10^5 s^{-1}. In the present study, the average $\dot{\gamma}$ at the highest flow rate (Re_p= 0.62) was about 1.2×10^4 s^{-1}. Thus, the effect of cell deformability could be neglected. Indeed, this was confirmed in Fig. 7, because the results of $PD_{6,\ \max}$ obtained from different Re_p cases overlapped and were plotted on a single curve in the figure.

The other factor possibly affecting the difference in migration length between rigid spheres and cancer cells is the variation in the size of the cancer cells. The migration length L_m, given by Eq. 2, is proportional to a^{-3}, where a is the radius of the particle. Thus, small variations in cancer cell size result in large differences in the migration length. For example, the migration length of a cancer cell with radius a_0 is double than that of a cancer cell with radius $1.26a_0$. The diameter distribution of the cancer cells used in this study is shown in Fig. 2, which may be, in general,

expressed by the Gaussian profile of probability density function (*PDF*):

$$PDF(d) = \frac{1}{\sqrt{2\pi\sigma}} \exp\left(-\frac{(d-d_0)^2}{2\sigma^2}\right), \quad (5)$$

where d is the diameter, d_0 is the average diameter, and σ is the standard deviation. The cumulative distribution function (*CDF*) in this case is

$$CDF(d) = \frac{1}{2}\left[1 + \mathrm{erf}\left(\frac{d-d_0}{\sqrt{2\sigma^2}}\right)\right]. \quad (6)$$

When $d=d_0$, $CDF=0.5$. Thus, half of the cancer cells have a migration length L_m greater than that of the rigid spheres. By substituting $d_0=15$ μm and $\sigma=4.3$ μm into Eq. 6, it can also be shown that 18% of cancer cells have a migration length more than double that of the rigid spheres.

The mixing effect due to RBC–RBC interactions was discussed in our previous studies (Lima et al. 2008b; Saadatmand et al. 2011). The results of these studies indicated that the diffusion coefficient D in non-dilute blood flow was approximately proportional to Hct and $\dot{\gamma}$, and $D = 3.6 \times 10^{-8}\mathrm{Hct}\dot{\gamma}\,\mathrm{m}^2/\mathrm{s}$, where $\dot{\gamma}$ is the average shear rate. The average mixing force F_m generated by the interactions between RBCs and a cancer cell can be estimated by simple scaling analysis. Let a cancer cell move randomly due to cell–cell interactions during the time duration of dt, and experience m collisions with displacement of about b in each collision. When there is no correlation between the collisions, the trajectory follows the standard random walk model, and the square displacement becomes mb^2. The average velocity of a cancer cell is mb/dt, which is equivalent to $6D/b$. Thus, F_m can be derived by exploiting Stokes' law, as $Fm = 36\pi\mu aD/b$. The shear-induced migration force F_s can be estimated as $F_s=8\rho U^2a^4/W_c$ (Bhagat et al. 2009). By taking the ratio of these two forces, we introduce a novel index β defined by:

$$\beta = \frac{F_s}{F_m} = \frac{2\rho U^2 a^3 b}{9\pi\mu D W_c^2}. \quad (7)$$

By substituting the physical quantities used in section 3.3 and assuming b is the RBC radius (i.e., $b=4$ μm), β can be calculated as $\beta=0.66/\mathrm{Hct}$. With Hct=0.1%, 1%, 10%, and 40% and $\mathrm{Re}_p=0.6$ as shown in section 3.3, β becomes 660, 66, 6.6, and 1.65, respectively. Clear migration of cancer cells was observed up to Hct=10%, in which the migration force was considerably larger than the mixing force. These simple scaling arguments can be useful to roughly estimate the effects of cell–cell interactions on the migration of particles.

5 Conclusions

We investigated the inertial migration of cancer cells in high hematocrit blood flow in microchannels. The migration of cancer cells in a dilute suspension was not as strong as that of rigid spheres, and the channel length required for cancer cell separation was about double that for rigid spheres. The low efficiency of cell migration was mainly due to the size variation of cancer cells. In non-dilute suspensions, cancer cells could migrate towards the equilibrium positions up to Hct=10%. At Hct=40%, however, clear migration of cancer cells was not observed due to the mixing effect of RBCs. We also performed simple scaling analysis to explain the experimental results, which captured the main features of the results. Thus, in designing a micro channel to separate cancer cells from a RBC suspension, the channel length has to be longer than that for rigid spheres and Hct has to be lower than 10%. These results are important for the design of microfluidic devices for separating cells from blood.

Acknowledgments This study was supported by Grants-in-Aid for Scientific Research (S) and (B) from the Japan Society for the Promotion of Science (JSPS; No. 19100008 and No. 22300149). We also acknowledge the support from the 2007 Global COE Program "Global Nano-Biomedical Engineering Education and Research Network Centre."

References

A.A.S. Bhagat, S.S. Kuntaegowdanahalli, I. Papautsky, Inertial microfluidics for continuous particle filtration and extraction. Microfluid Nanofluid **7**, 217–226 (2009)

G.T. Budd, M. Cristofanilli, M.J. Ellis et al., Circulating tumor cells versus imaging-predicting overall survival in metastatic breast cancer. Clin. Cancer Res. **12**, 6403–6409 (2006)

D.D. Carlo, Inertial microfluidics. Lab Chip **9**, 3038–3046 (2009)

D.D. Carlo, J.F. Edd, D. Irimia et al., Equilibrium separation and filtration of particles using differential inertial focusing. Anal. Chem. **80**, 2204–2211 (2008)

M. Cristofanilli, G.T. Budd et al., Circulating tumor cells, disease progression, and survival in metastatic breast cancer. N. Engl. J. Med. **351**, 781–791 (2004)

M. Cristofanilli, D.F. Hayes, G.T. Budd et al., Circulating tumor cells: A novel prognostic factor for newly diagnosed metastatic breast cancer. J. Clin. Oncol. **23**, 1420–1430 (2005)

D.R. Gossett, W.M. Weaver, A.J. Mach et al., Label-free cell separation and sorting in microfluidic systems. Anal. Bioanal. Chem. 397, 3249–3267 (2010)

S.C. Hur, H.T.K. Tse, D.D. Carlo, Sheathless inertial cell ordering for extreme throughput flow cytometry. Lab Chip **10**, 274–280 (2010)

T. Ishikawa, H. Fujiwara, et al., Asymmetry of blood flow and cancer cell adhesion in a microchannel with symmetric bifurcation and confluence. Biomed. Microdevices. **13**, 159–167 (2011)

S.S. Kuntaegowdanahalli, A.A.S. Bhagat et al., Inertial microfluidics for continuous particle separation in spiral microchannels. Lab Chip **9**, 2973–2980 (2009)

G.Y.H. Lee, C.T. Lim, Biomechanics approaches to studying human diseases. Trends Biotechnol. **25**, 111–118 (2007)

R. Lima, S. Wada et al., *In vitro* blood flow in a rectangular PDMS microchannel: experimental observations using a confocal micro-PIV system. Biomed. Microdevices **10**, 153–167 (2008a)

R. Lima, T. Ishikawa et al., Radial dispersion of red blood cells in blood flowing through glass capillaries: The role of hematocrit and geometry. J. Biomech. **41**, 2188–2196 (2008b)

J.S. Park, S.H. Song, H.I. Jung, Continuous focusing of microparticles using inertial lift force and vorticity via multi-orifice microfluidic channels. Lab Chip **9**, 939–948 (2009)

E.D. Pratt, C. Huang, B.G. Hawkins, et al., Rare cell capture in microfluidic devices. Chem. Eng. Sci. **66**, 1508–1522 (2011)

M. Saadatmand, T. Ishikawa et al., Fluid particle diffusion through high-hematocrit blood flow within a capillary tube. J. Biomech. **44**, 170–175 (2011)

S. Suresh, Biomechanics and biophysics of cancer cells. Acta Mater. **55**, 3989–4014 (2007)

Z. Wu, B. Willing, J. Bjerketorp et al., Soft inertial microfluidics for high throughput separation of bacteria from human blood cells. Lab Chip **9**, 1193–1199 (2009)